UCID- 20289

PRELIMINARY EVALUATION OF ALTERANT GEOPHYSICAL TOMOGRAPHY IN WELDED TUFF

A. L. Ramirez
W. D. Daily

December 1984

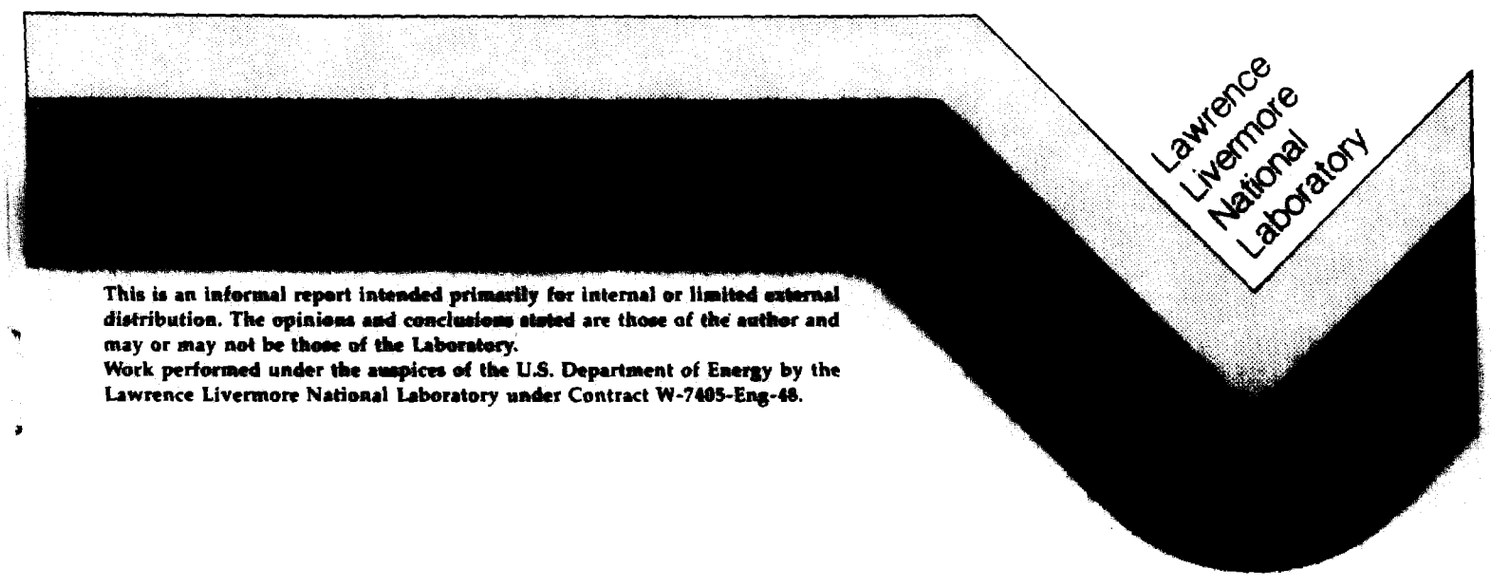

Work performed under the auspices of the U.S. Department of Energy by the Lawrence Livermore National Laboratory under Contract W-7405-Eng-48.

TABLE OF CONTENTS

Page

Abstract iii

1. Introduction.....1

2. Experimental Concept.....3

3. Experimental Procedure.....5

3.1. Pre-experiment Inversion Simulations.....5
3.2. Geologic Setting.....8
3.3. Data Collection.....10

4. Experimental Results and Discussion.....12

4.1. Geophysical Tomographs.....12
4.2. Alterant Geotomographs.....16
4.3. Other Geological Data.....20
4.4. Analysis of Data Noise.....26
4.5. Possible Flow Paths.....29

5. Summary and Conclusions.....31

Acknowledgements.....34

References 35

Appendix 38

ABSTRACT

In-situ electromagnetic measurements have been performed at 300 MHz to evaluate the applicability of alterant geophysical tomography to delineate flow paths in a welded tuff rock mass. The measurements were made before, during and after a water-based tracer flowed through the rock mass. Alterant geophysical tomographs are compared with independent evidence--borescope logs, neutron logs and dyed rock samples. Anomalies imaged in the tomograph match fractures mapped with the borescope. The location of tracer-stained fractures coincides with the location of some image anomalies; other geophysical anomalies exist where tracer-stained fractures were not observed, perhaps due to poor core recovery. Consequently, a conclusive evaluation of the technique's effectiveness is not possible at present. Additional work is planned to conclusively evaluate the capabilities of alterant geophysical tomography in an environment similar to the Waste Package Environment Tests expected in Yucca Mountain.

1. INTRODUCTION

The Nevada Nuclear Waste Storage Investigations (NNWSI) Project is studying the suitability of the tuffaceous rocks at Yucca Mountain, Nevada Test Site, for the construction of a high-level nuclear waste repository. Lawrence Livermore National Laboratory (LLNL), Livermore, California, has been given the task of designing and verifying the performance of waste packages for the NNWSI Project.

The properties of the geologic environment around a nuclear waste repository must be well characterized so that repository performance can be reliably predicted. Many geologic factors controlling the properties of this barrier are strongly interrelated. For example, groundwater flow through fractures and/or pores will impact the chemical and physical properties of the geologic barrier and, hence, its containment capacity. Fractures are often the predominant flow paths and, therefore, are the focus of many experimental programs.

Various in-situ tests will be conducted within the Topopah Springs member of the Paintbrush Tuff at Yucca Mountain to investigate its behavior in the vicinity of simulated waste packages. The planned tests will simulate the repository environment by emplacement of heaters within the rock mass. Rock behavior will be monitored during the heating and cooling phases and with water percolating through the rock mass. A key objective of this work is to study the hydrologic behavior of the rock under a thermal load.

The interaction of the groundwater with the simulated waste package and rock will be studied with various measurement techniques. This document

discusses the preliminary results of an experiment in which one of the candidate measurement techniques, alterant geophysical tomography, (Ramirez and Lytle, 1983) was used to investigate in-situ fracture flow. Specifically, our objective was to use alterant tomography to delineate flow paths and identify the specific fractures or fracture systems conducting water in the rock mass. Results from this experiment were compared with neutron logs, borescope surveys and post-experiment core samples.

Previous work under different geologic conditions has suggested that geophysical tomography can delineate in-situ fracture flow and map rock mass porosity. At a fractured granite site near Oracle, Arizona, fully saturated fractures could be identified in tomographs and their locations correlated with fracture location along the borehole as inferred from well log data (Ramirez et al., 1982). These same tomographic data were used in conjunction with laboratory data which related rock water content to the electromagnetic parameters measured in the tomography to generate a two-dimensional map of water content and, therefore, total porosity of the rock mass (Daily and Ramirez, 1984).

These same techniques can be used to study the hydrologic characteristics of densely welded tuff. However, differences in the geologic setting and experimental constraints between the granite and tuff sites are substantial, so that another objective of the experiments reported herein was to identify and deal with these differences. One of the important differences between granite and tuff is rock porosity. For example, typical porosity values are 14 percent for tuff and 0 to 1 percent for granite (Goodman, 1980). Other conditions being equal, tuff is likely to have a substantially larger water

content than granite. Increases in the water content caused by the presence of fractures will be relatively larger in granite due to its lower matrix porosity. Thus, it is easier to detect water-filled fractures in granite because the contrast between the matrix and the fractures will be substantially greater than in tuff.

2. EXPERIMENTAL CONCEPT

Geophysical tomography is conceptually similar to medical tomography which inspired it (Kuhl and Edwards, 1963, Lager and Lytle, 1977). An underground region is sampled by transmitting energy through it along many paths having multiple orientations. The transmitted signal must be influenced by the property of interest in the region. Then the signal parameter of interest is inverted to yield a map of the parameter. Finally, the property of interest is inferred from this map based on some conceptual model which relates the measured parameter and the property.

For this study, we used measurements of very high frequency (VHF) electromagnetic energy. We assume that this energy is transmitted along straight ray paths between two boreholes and the signal attenuation between the transmitter and receiver is measured along each ray path. In situ measurements of the real part of the dielectric constant (ε_r) of the rock mass show that it is relatively constant. Since propagation velocity is a function of ε_r we expect no significant changes in propagation velocity and therefore minimal ray bending.

The region between the boreholes is divided into many cells and an attenuation rate is calculated for each cell from line integral equations which can be written for each ray path. This set of equations can be solved iteratively using the algorithm SIRT (Lager and Lytle, 1977) for the attenuation rates (defined as the inverse of the distance along which the signal is attenuated by a factor of 1/e) of each cell. All tomographs in this report are constructed with 10 iterations. This array of cells is a two-dimensional map of the electromagnetic attenuation rate in the plane between the boreholes. An image of the attenuation rate is constructed by assigning a gray level to each cell based on its attenuation rate.

In practice it is often desirable to use three coplanar holes. The signal is transmitted from one of the outside holes and received along the same ray path in the other two. The difference in the two received signals defines the attenuation between the two receiver boreholes. Although this technique requires an additional borehole, it has some advantages. It eliminates the need to know the transmitter radiated power, transmitter gain, and receiver effective areas or radiation patterns. In other words, the data are independent of these system parameters. In practice, these parameters are difficult to measure accurately or maintain constant over long time periods. Our experiment was designed to use this differential measurement technique because measurement accuracy and temporal stability were important. A detailed description of the method is given in the Appendix.

A geotomograph is a map of electromagnetic attenuation. It is of interest only insofar as it relates to some property of importance to

repository performance. Fortunately, rock mass electromagnetic attenuation rate is a sensitive function of (among other things) water content of the rock (Poley, et al., 1978; Daily and Ramirez, 1984). Typically, the larger the water content, the larger the attenuation rate. However, there are other formation properties (e.g., lithology) affecting electromagnetic parameters to a lesser extent. Thus, we used a technique known as alterant geophysical tomography (Ramirez and Lytle, 1983) where measurements are made before and after a tracer of controlled electrical properties is added to the rock. The image formed by subtracting values of corresponding cells of the "before" and "after" tomographs is the alterant tomograph. Rock influenced by the tracer is represented in the alterant image by the changes in attenuation rate. Thus, alterant tomography might be useful to define flow paths by distinguishing between water entering the rock along fractures or through the matrix and invariable anomalies such as those caused by water trapped in the matrix.

3. EXPERIMENTAL PROCEDURE

3.1. Pre-experiment Inversion Simulations

Pre-experiment computer simulations showed that the proposed tomographic inversion method could resolve the relatively small differences in electrical properties expected to result from fracture flow. Figure 1 presents the ideal target used for the simulation. The model incorporates our expectations for the electrical properties of the rock mass.

Vertical fractures are used in the model because available information (Winograd and Thordarson, 1975; Langkopf and Eshom, 1982) indicated that the fractures in welded tuff are predominantly vertical cooling joints. Lenses are characterized by a high electromagnetic attenuation rate (1.5 m^{-1}), to represent rock with relatively high moisture content (the attenuation rate is the inverse skin depth or one over the distance the signal is attenuated by a factor of e = 2.72). These lenses are embedded in regions having a low (0.3 m^{-1}) attenuation factor representing rock of lower moisture content. When water is introduced into the fractures, we assume that the electrical properties of the fractures change (1.0 m^{-1} - "dry" case; 1.05 m^{-1} "wet" case) but that the surrounding rock remains unchanged because of very low permeability. This was done to test the capability of the inversion method to resolve small changes in attenuation factor caused by fracture saturation in the presence of highly attenuating rock (lenses). The values of attenuation rate chosen for each component of the model were based on laboratory measured values from rocks of similar composition and porosity.

Figure 1 shows the results of simulations where tomographs, both with data sets which are noise free for the "dry" and "wet" cases, were generated and subtracted from each other. These results show that if relatively noise-free data are available the inversion method used can resolve fractures with small changes in the electrical properties even when embedded in high attenuation features in the rock.

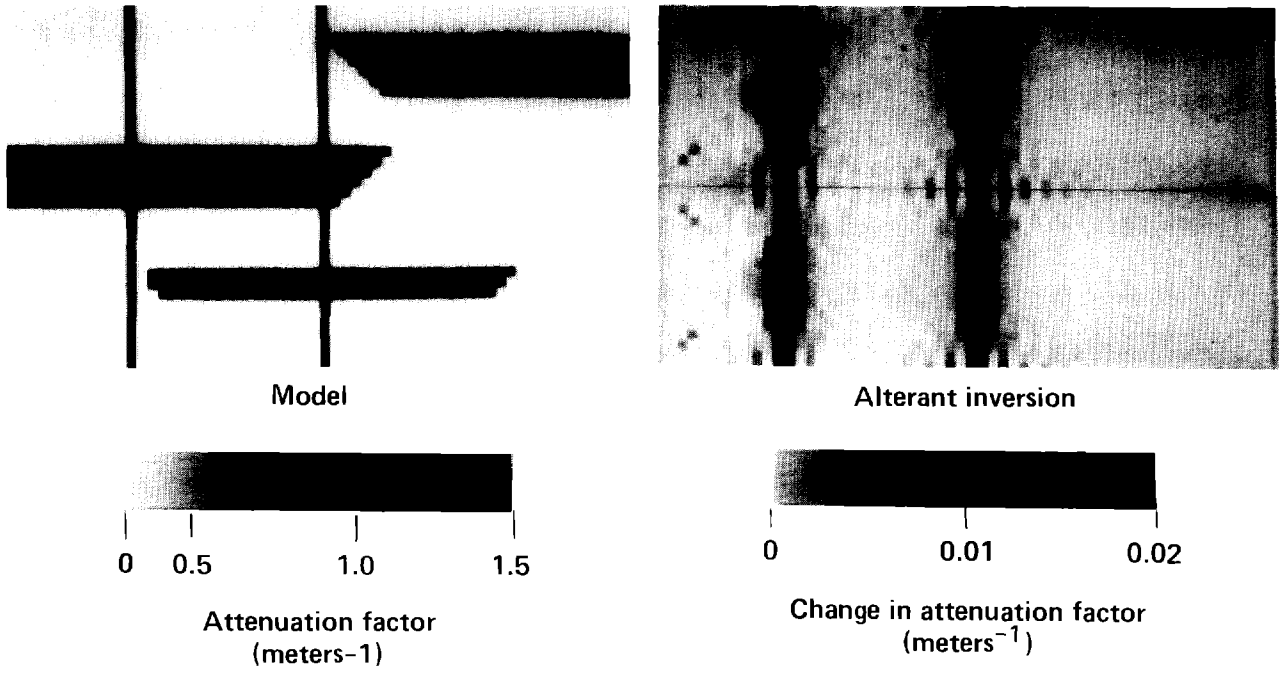

Figure 1. A model of electromagnetic attenuation distribution in a hypothetical rock mass. The horizontal features in the model on the left represent lenses and the vertical bands represent water-filled fractures. Attenuation factor is the inverse skin depth for the electromagnetic wave. Synthetic tomographs of the model with the fractures at 1.0 and 1.05 m^{-1} were subtracted to generate the alterant inversion shown on the right.

3.2. Geologic Setting

The experiment was conducted in an ash flow tuff formation of the Grouse Canyon member of the Belted Range Tuff because this formation is readily accessible and is lithologically similar to that of the proposed repository horizon, the Topopah Spring tuff, at Yucca Mountain. The Grouse Canyon tuff exposed in G-tunnel is a partially to densely welded tuff striking N55° E and dipping 9° W (Langkopf and Eshom, 1982). This formation is in the unsaturated zone but has a degree of saturation greater than 85 percent. Porosity ranges from 13 to 25 percent (Johnstone and Wolfsberg, 1980). The measurements of electromagnetic attenuation rate were made between three parallel coplanar boreholes drilled 90 centimeters apart into the rib of the extensometer drift in the G-tunnel complex at the Nevada Test Site. Figure 2 shows the borehole layout relative to the drift. Boreholes 2, 3 and 4 serve as measurement holes. Borehole 1 is drilled 2 degrees below horizontal to provide a reservoir from which water could infiltrate the rock. All boreholes are six meters long. This borehole layout and scale is similar to that planned for the simulated waste package tests to be conducted in Yucca Mountain.

The top of a rubble zone is located about 30 cm below the collar of hole 4. This zone marks the transition between welded tuff, above, and nonwelded tuff, below. Based on data from Langkopf and Eshom (1982) we infer a zone of moderately welded tuff about two meters thick directly above this rubble. Although there is a gradational contact between the moderately welded and the densely welded tuff above it, note that the tomographic plane between boreholes 3 and 4 is largely within moderately welded tuff while the plane between holes 2 and 3 is predominantly within densely welded tuff.

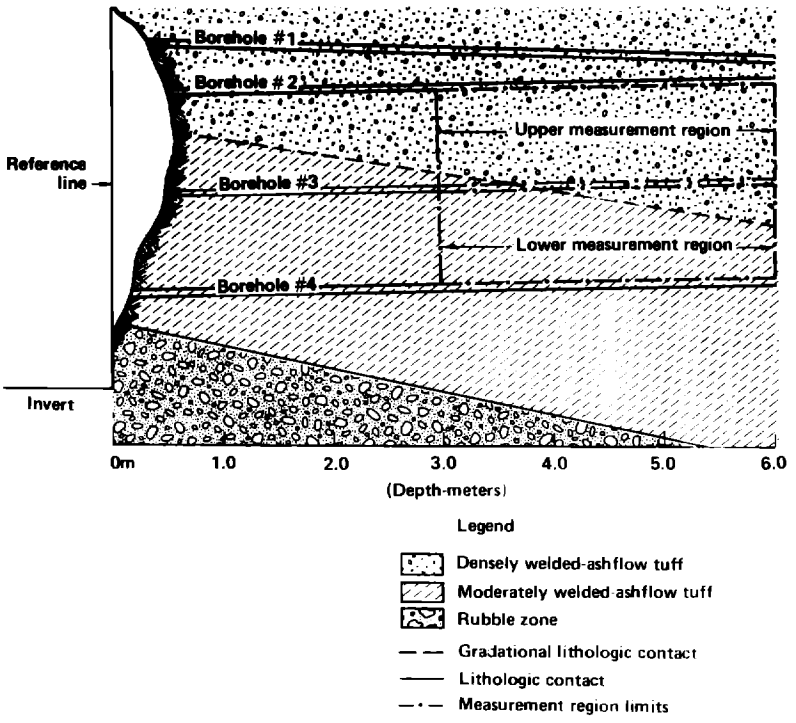

Figure 2. Borehole layout and tomographic plane relative to local geology (geology extrapolated from map by Langkopf and Eshom (1982) pp. 15-16).

A vertical fault intersects all the boreholes at a depth of about two meters with an angle of about 30 degrees between fault plane and borehole axis. This fault has an aperture in some locations exceeding one centimeter. The rock also contains numerous smaller fractures. Previous fracture mapping near this region of G tunnel indicates that most fractures are nearly vertical with two predominant sets striking approximately N40-60°W and N20-40°E. The azimuth of our measurement boreholes is N15°W.

3.3. Data Collection

Differential tomographs were made between holes 2 and 3 (referred as the upper measurement region) and between holes 3 and 4 (lower measurement region). The tomographs image the region along the holes between three and six meter depth (measured laterally). All depth distances were measured from a reference line just outside the hole collars. The images from both the upper and lower measurement regions, represent a combined region 180 cm high and 300 cm long. Hot air was forced into the boreholes during the two weeks prior to the experiment in an attempt to drive from the fractures as much drilling water as possible.

The data collection procedure was similar in all cases: (1) 931 ray paths were sampled by moving antennas in the holes 2 and 4 at intervals of 10 cm (hole 3 antenna is positioned on the ray connecting the other antennas); (2) the field hardware and data collection system were similar to that described by Daily et al. (1982); (3) the three antennas were specially designed sleeve dipoles, 20 cm in overall length; (4) the signal frequency was 300 MHz.

Initial measurements between boreholes 2 and 3 and between 3 and 4 were made prior to the start of tracer flow. Inversions of these measurements provide the baseline attenuation factor geotomographs of the rock and are designated as "before" measurements. Then borehole 1 was filled with a solution of mine water and methylene chloride dye which stains the rock dark blue on contact. Coring the rock mass was planned as the last part of the experiment to locate blue fractures and corroborate the tomographic data. Data collection for a tomograph was started in the upper measurement region within a few minutes after the tracer was added to hole 1. Subsequently, measurements were taken for a tomograph nearly every weekday for the next two calendar weeks alternating each day between the upper and lower measurement regions. These sets of measurement are designated "after" measurements. Borehole 1 was kept filled during this entire period with either mine water (dc electrical conductivity 2.1×10^{-2} S/m) or dye solution mixed at about 10 g methylene blue per 55 gallons of water (dc electrical conductivity 2.2×10^{-2} S/m). The differences in electromagnetic properties between the tracer and the natural pore water of the formation are unknown. The above series of tomographs, 10 in all, was made in an attempt to detect tracer movement rates in the formation.

Tracer infiltration was terminated and the formation allowed to drain for two weeks. Following this, measurements (designated as "drained measurements") were made of both the upper and lower regions. Finally, a salt water and dye tracer solution (dc electrical conductivity 2.1×10^{-1} S/m) was added to borehole 1 and allowed to infiltrate the formation for three days. Three data sets were then collected of the upper and lower measurement regions.

Additional geophysical information on the rock mass was collected in an effort to corroborate our inferences from the tomographic data. Neutron surveys were made to obtain overall rock mass saturation and to locate those fractures which accepted water. These surveys were made in holes 2, 3, and 4 before the unsalted water was added to the formation and again after the geotomographic data was taken when water had been infiltrating in the formation for more than two weeks. In addition, boreholes were cored in the plane imaged by the geotomographs to locate fractures stained by the blue dye and therefore identify the location of those fractures which conducted water. Two holes were cored between each of the three tomographic measurement holes after the tomographic data was collected. Also, a borescope was used to log fractures in holes 2, 3, and 4, and the four post-experiment core holes.

4. EXPERIMENTAL RESULTS AND DISCUSSION

4.1. Geophysical Tomographs

Figure 3 presents inversions of the absolute attenuation factor of the upper measurement region at various stages of the experiment. Each of the images shown in this and subsequent sections consist of an array of 7.5 cm square cells 40 rows long and 12 columns high. The gray scale represents the inverted values of attenuation factor with dark gray tones corresponding to high attenuation factors. Regions of the rock with a relatively high moisture content are known to have a high attenuation factor.

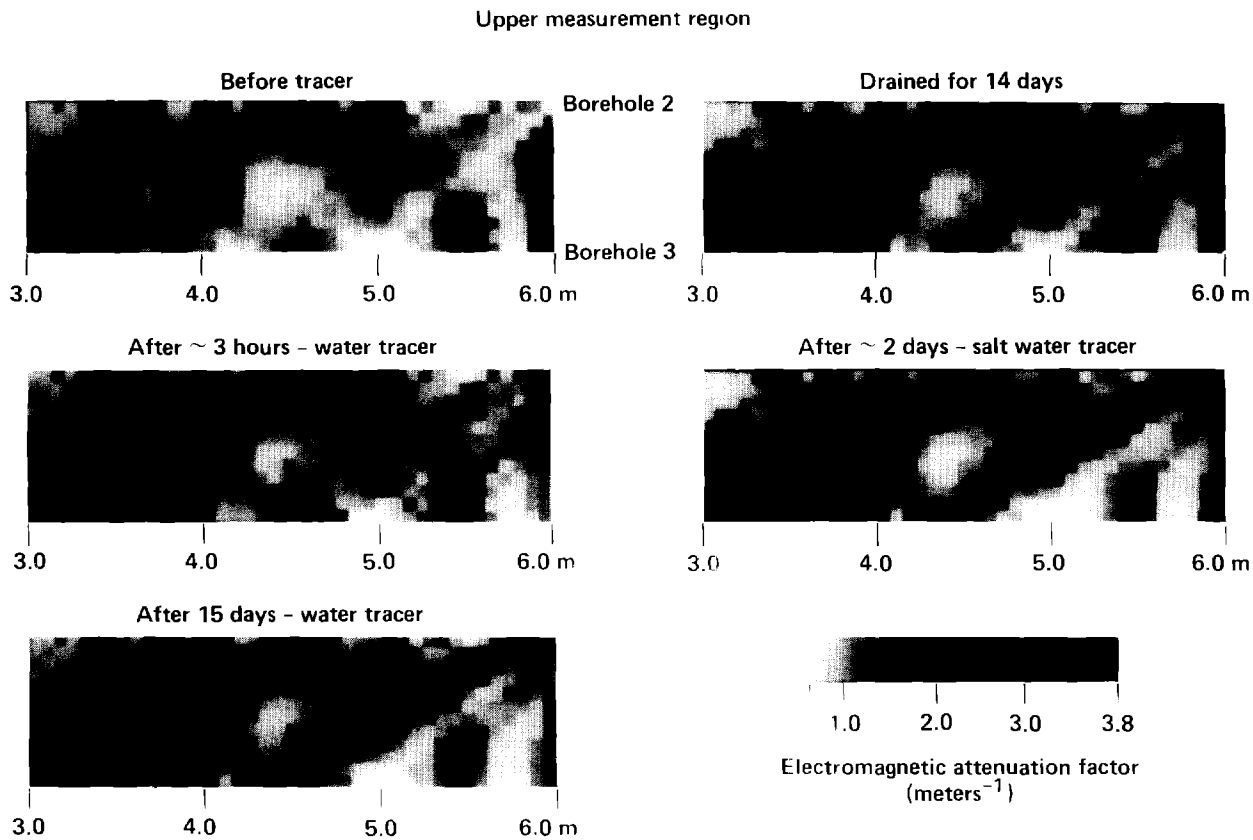

Figure 3. Geotomographs of the upper measurement region at various stages in the experiment. Attenuation rate increased gradually with time as water permeated the rock mass. Allowing water to drain from the formation for 14 days apparently does not restore the rock to its original degree of saturation. Introduction of higher electrical conductivity tracer, salt water, increases rock mass attenuation to values somewhat higher than that achieved by mine water saturation.

The attenuation factor for the inversions shown in Fig. 3 remain approximately constant throughout most of the region--the images largely duplicate each other. However, localized sectors of the rock show slight increases in attenuation (some image cells become slightly darker) as the saturation of the rock mass increases. These changes are consistent with our general expectations: (1) changes are confined to localized regions of the rock mass--probably fractures, and (2) changes caused by increasing the saturation of a fracture are small compared to bulk attenuation of the rock mass.

Figure 4 presents images of the upper and lower measurement regions in the same spatial relation as the rock mass they represent. The upper photograph shows the "before" case. The average attenuation factor of the upper and lower regions is 1.43 m^{-1} and 1.51 m^{-1} respectively--nearly the same. The imaged structure along the common boundary between these two regions is consistent. Figure 4b shows a similar comparison for the "after case (rock mass had received the water tracer continuously for 15 days). The average attenuation for these two regions is 1.49 m^{-1} and 1.14 m^{-1} for the upper and lower regions respectively--clearly different. This difference is not representative of changes in rock properties. We have determined that it is most likely an artifact of antenna characteristics. Post-experiment calculations show that the impedance of one antenna changed when water entered the rock mass, and resulted in an artificial bias in attenuation rate for all cells in images of the lower region. This antenna behavior is expected when the electrical environment changes (Lytle, 1984). The consequences are usually negligible because the antenna is used at a frequency well below its

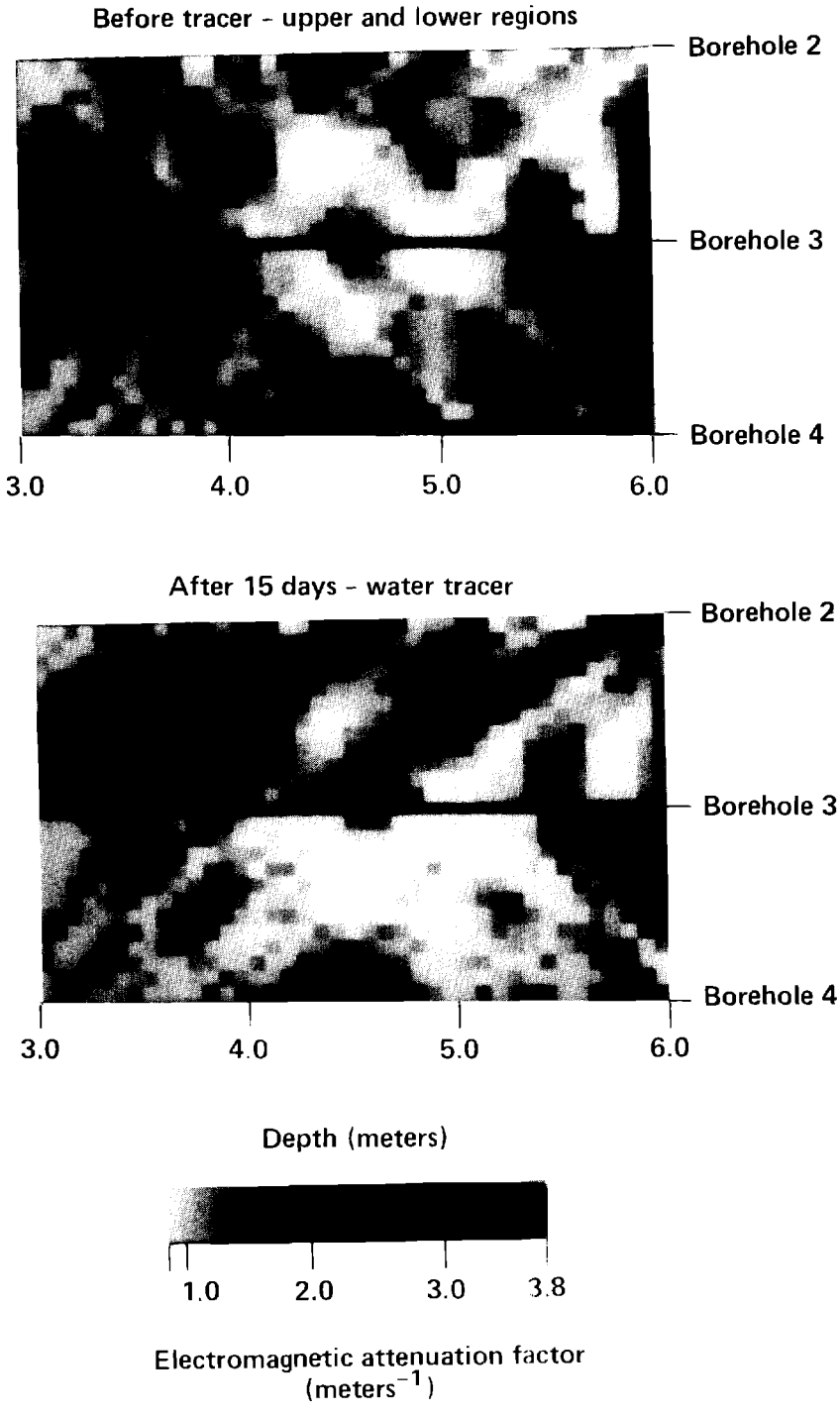

Figure 4. Geotomographs of the entire image plane before and after mine water tracer was introduced into the rock.

resonant frequency so that the antenna impedance is insensitive to changes in the environment. For this experiment we chose to operate near antenna resonance to obtain maximum efficiency. In retrospect it is apparent that measurements made at a frequency sufficiently below 300 MHz will eliminate this effect. Tomographs for the upper measurement region (Fig. 3) are internally consistent. This fact as well as measurements of antenna performance during the experiment indicate stable antenna impedance for this data. Therefore, we believe that all tomographs shown in this report except the lower one in Fig. 4 are free of antenna artifacts.

Figure 5 compares the upper and lower regions while salt water flowed through the rock. The average inverted values for the two regions are the same; 1.58 m^{-1}. These data were largely unaffected by antenna impedance changes and, thus, accurately represent the electromagnetic properties of the rock mass. Measurements of antenna properties during the experiment show that salt water (which has electromagnetic properties different from fresh water) stabilized the antenna impedance.

4.2. Alterant Geotomographs

Computer simulations presented in Section 3.1 show that one of the primary advantages of alterant tomography is its capability to resolve relatively small changes in attenuation factor (tracer in a narrow fracture) embedded in a highly attenuating background (highly saturated rock mass). This section shows the in-situ changes in attenuation factor of the rock mass caused by introduction of the water. The alterant tomographs are differences

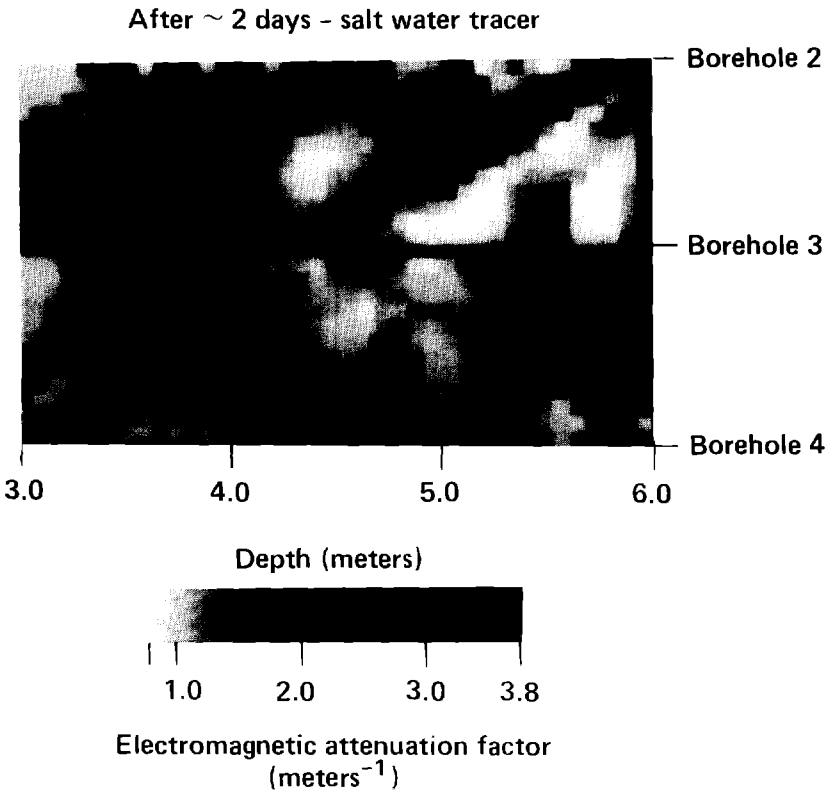

Figure 5. Geotomograph of the image plane after salt water tracer was added to the formation.

in attenuation factor between an "after" inversion tomograph and its corresponding "before" inversion. We call these inversions "alterant tomographs" because they should show only the alterations caused by the water and salt water tracers and reject other structure in the images having constant attenuation rates.

Figure 6 compares alterant tomographs showing the changes in attenuation factors caused by the water and salt water tracers. The upper image shows changes in the rock mass 15 days after water tracer was introduced. The lower image shows changes relative to the drained inversion caused by the salt water tracer approximately 2 days after the flow began. The general shape and location of anomalies are similar in these two images. As expected, the attenuation rate changes of the anomalies were larger with the higher conducting salt water in the formation than with the mine water tracer in the formation. The two vertical anomalies between boreholes 2 and 3 centered at depths of 3.4 m and 3.9 m may be water-filled fractures. This interpretation is consistent with geologic data (Langkopf and Fshom, 1982; Winograd and Thordarson, 1975) that most of the fractures in this unit are vertical. A diagonal anomaly beginning at a depth of 4.0 m in borehole 3 is present in both cases. This anomaly suggests flow paths other than vertical in the rock mass. This particular anomaly will be discussed more completely in Section 4.4.

Figure 6 implies a more complex network of fractures in the lower measurement region. From four and a half to six meters depth, especially near borehole #4, the tomograph shows a broad region where image cells have a checkerboard appearance. A possible explanation for this checkerboard

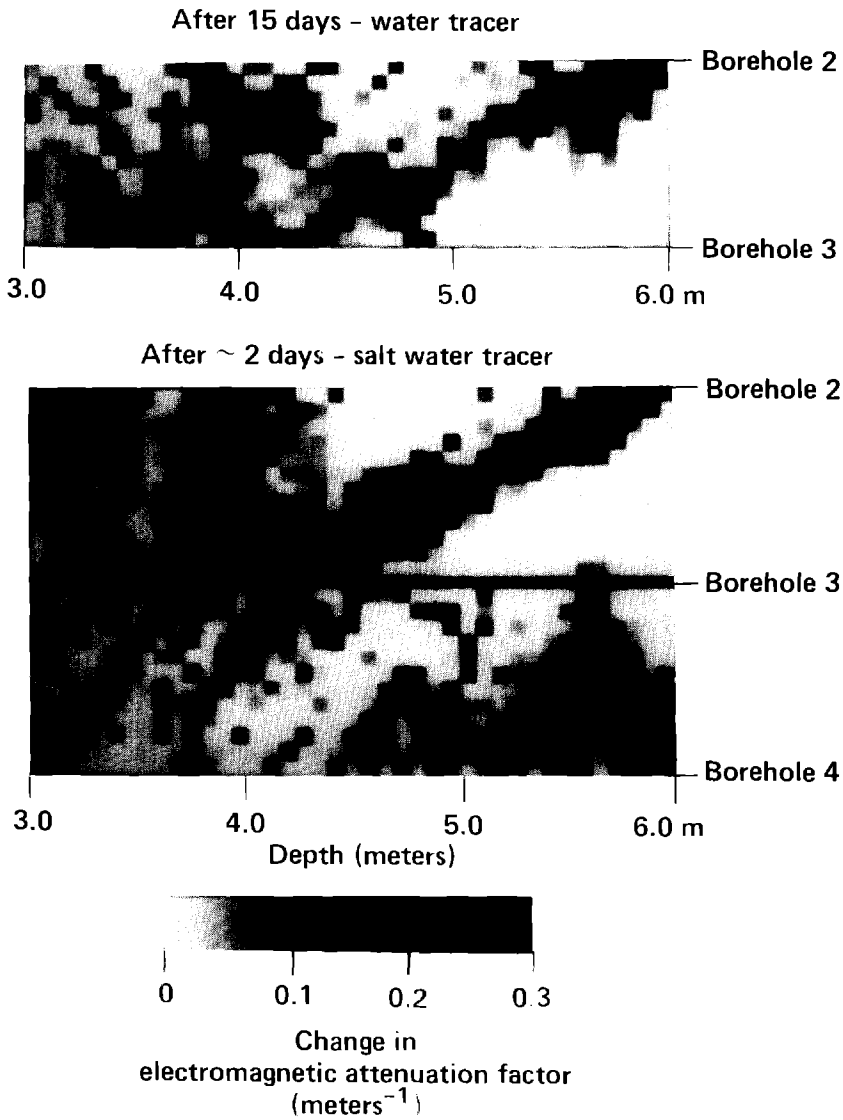

Figure 6. Alterant tomographs constructed by subtracting the attenuation rate of cells in the tomograph made before water was added to the rock from that of corresponding cells in the tomograph made after tracer was added to the rock.

appearance is that it represents a complex network of closely spaced flow paths (dark image cells) isolated by impermeable rock matrix (light image cells). However, identifying individual fractures is not possible with these tomographs. From three to four meters depth in the lower measurement region, the tomographs imply a less complex picture with some isolated near-linear features suggestive of separate flow paths. This interpretation is discussed below when the tomographs are compared to fractures mapped in the measurement plane.

4.3. Other Geological Data

Other geological data were also collected in the rock mass to evaluate the validity of the tomographs. The neutron logs made when the rock was dry, and then again when saturated, are presented in Fig. 7. The logs of borehole 2 show a small increase in count rate in the saturated formation all along the borehole. This increase implies a higher water content in the rock mass. The reservoir borehole used to introduce water into the formation was only 23 to 25 centimeters from borehole #2. Telford et al. (1976) report that the radius of influence of neutron tools ranges from 17 centimeters in porous formations to 60 centimeters in low porosity rocks, and, therefore, this modest increase in the neutron log probably reflects only the presence of the water standing on hole 1. The logs of borehole 3 show little or no change in saturation at most locations and decreases in saturation at 5.0 and 5.5 meters. Borehole 4 shows moderate increases at three and four meter depths.

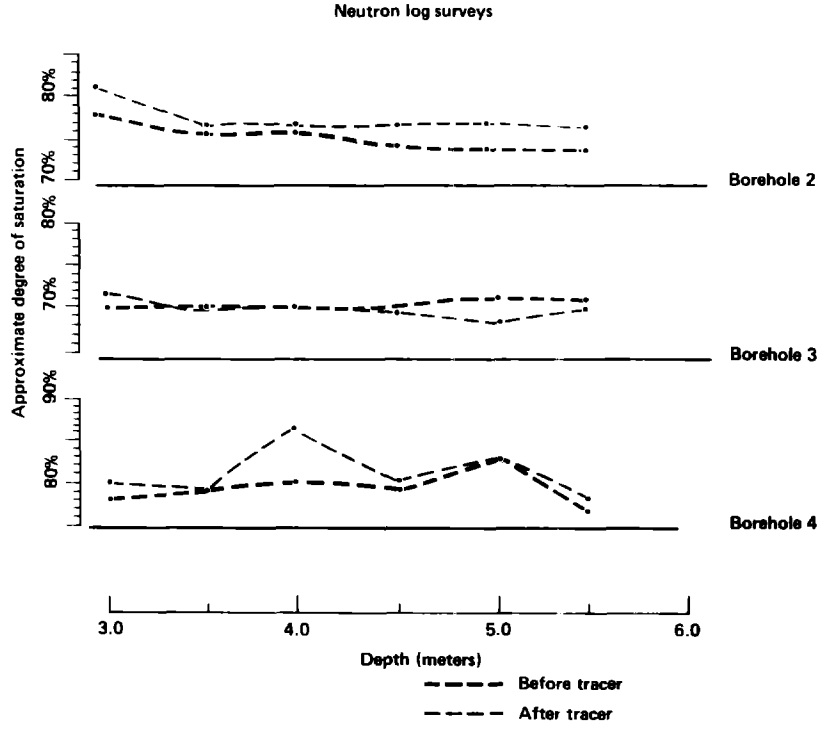

Figure 7. Neutron logs of boreholes 2, 3 and 4. The approximate degree of saturation is an average value around the probe over a spherical volume with perhaps a half meter radius.

In the upper measurement region, the neutron logs show no evidence of the flow paths imaged by the tomographs. Therefore, we believe that the increased saturation sensed by the neutron log in hole 4 at 4 m depth does not correlate with a tomographic anomaly at that position, but rather, results from a relatively large water concentration somewhere outside the image plane. The flow paths imaged by tomography do not appear in the neutron log data probably because the water content in isolated fractures is small compared to the water content in the pore volume. The porosity of G-tunnel Grouse Canyon tuff ranges from 13-25 percent with the saturation greater than 85 percent (Johnstone and Wolfsberg, 1980). Assuming a 20 percent porosity, and an 85 percent saturation, the pore water volume is 17 percent of the rock volume whereas water-filled fractures with a 0.1 millimeter aperture and spacing of 10 cm add only 1/10th percent water by volume to the rock mass. Therefore, the increased water along a fracture will change only slightly the water content of the rock in a rock mass with an already high degree of saturation. These changes are below the sensitivity threshold of the neutron tool (Schuck, personal communication). Decreases in the degree of saturation shown in Fig. 7 also provide support to this argument since it is unlikely that the degree of saturation of the rock mass would decrease during the 15 day period during which water tracer flowed through the rock mass.

Core recovery from the post experiment coring is shown in Fig. 8. We note that even for those core runs where 100 percent recovery is indicated, the core sustained damage. Many of the fracture surfaces were polished and rounded from spinning against other pieces in the barrel.

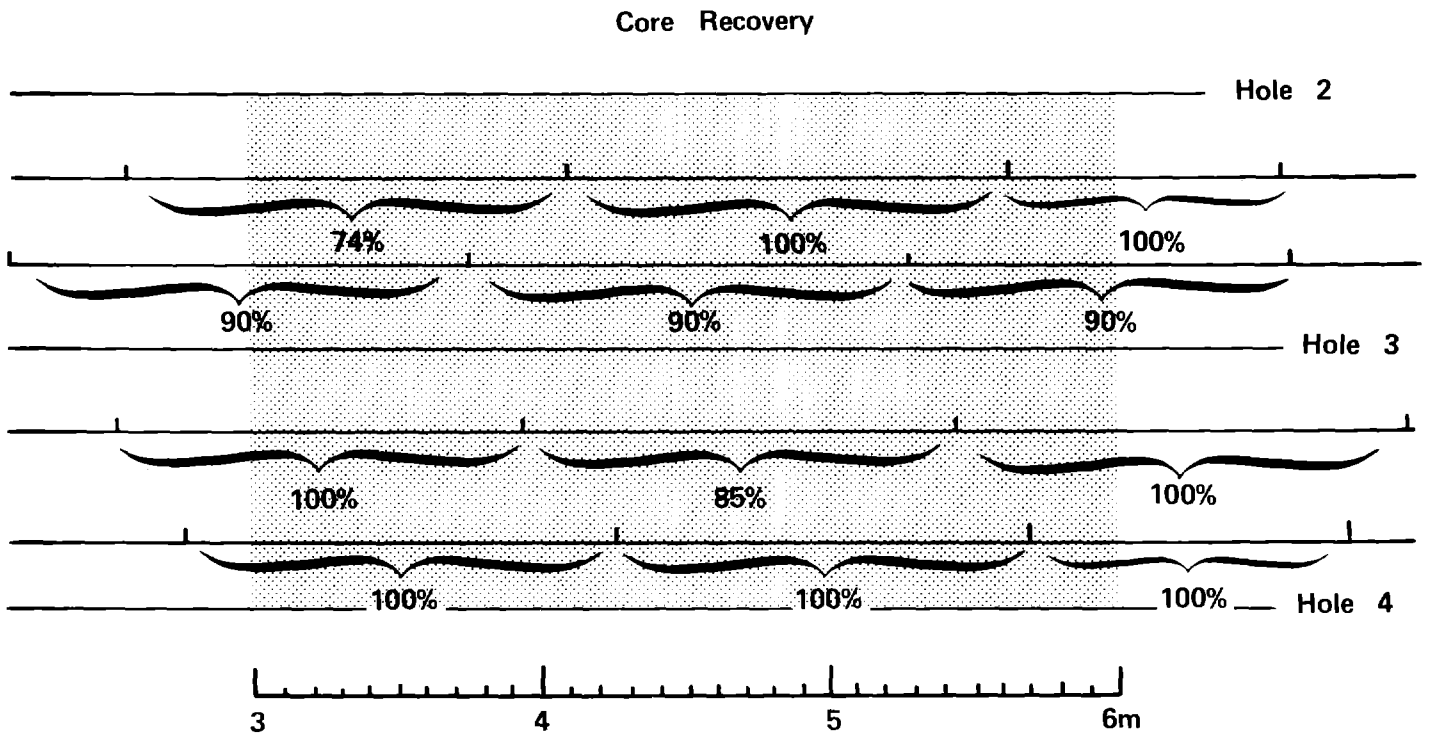

Figure 8. Core recoveries obtained along the post-experiment holes. All of the core was broken into pieces having an average length of about 7 cm. Many of the core faces exhibited damage caused by spinning inside the barrel. The shaded portion indicates the measurement region.

Post-experiment borehole data and borescope survey data are presented in Fig. 9a. This figure shows the range of depths along which the recovered dyed samples could have been located as determined by the length of unrecovered core for the corresponding drill run. The alterant tomograph is also shown in Fig. 9. Several conclusions are possible from the comparison of the alterant tomograph and other geological data:

- The location ranges of the three dyed core pieces match the location of three image anomalies.

- Several image anomalies coincide with fractures detected by the borescope surveys.

- No blue-stained core was recovered from regions where the tomographs indicated absence of flow paths.

- Several anomalies in Fig. 9 occur along regions where no dyed samples were recovered.

The last conclusion may mean that: (a) No tracer flow occurred at locations where image anomalies are observed or, (b) the drilling process destroyed the dye coating the fracture surfaces. At present, we favor the latter explanation for the following reasons. All of the recovered core was broken into small pieces, and some of the core was entirely destroyed by the drilling. Core recoveries ranged from 74 to 100 percent and, in fact, in the

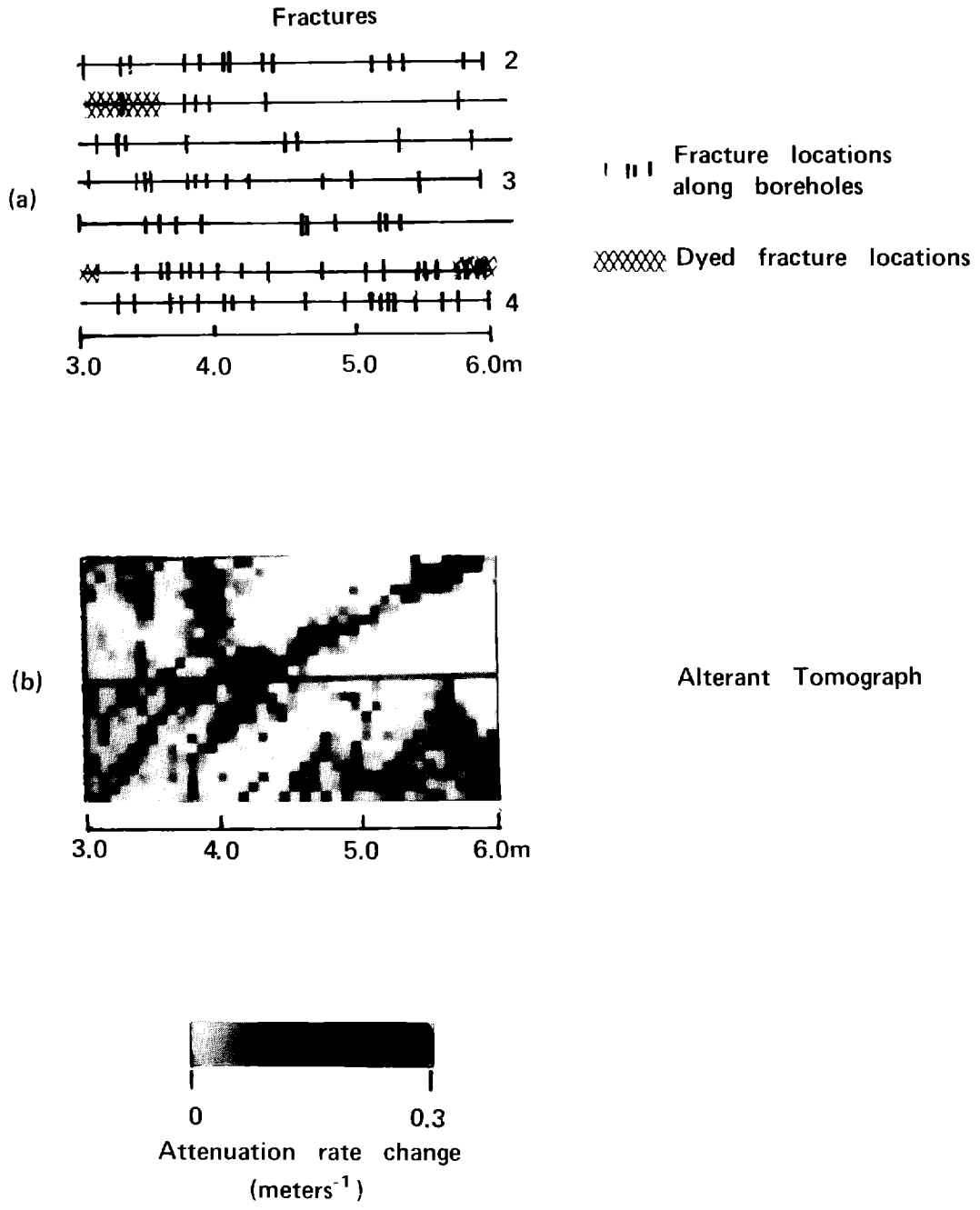

Figure 9. Comparison of an alterant tomograph, fracture location data, and the locations of recovered dyed fractures.

upper region, the two vertical anomalies at depths of 3.5 and 4.2 meters occur where sections of core are missing. The parts of the cores most likely to be destroyed are fracture surfaces where sections of core on either side of the fracture rotate relative to each other inside the core barrel. The majority of core faces observed are rounded and polished by this process even where 100 percent recovery was obtained. Dye coating the fracture surface could have been destroyed because it coats only the fracture surfaces and does not penetrate the matrix.

4.4. Analysis of Data Noise

An important element controlling the reliability of the alterant tomographs shown in Fig. 9b is data noise. The relatively small changes shown by the images are obtained by subtracting two data sets consisting of relatively large numbers. Thus, slight errors in large numbers could account for some of the changes. We have estimated the errors present in the data from which the tomographs were constructed and then used computer simulations to investigate how these errors propagate in the alterant tomographs. In this manner, we have discarded anomalies which could have been associated with measurement error.

Measurement noise was estimated by comparing two data sets (subsequently used for tomographs) taken 16 hours apart while the rock mass properties remained constant. The differences between corresponding measurements were used as the error estimates. A plot of the errors suggested that they were normally distributed and their mean and standard deviations were

therefore used to characterize the distribution. Computer simulations were then used to estimate the effects of these errors on the alterant tomographs. The "before" and "after" reconstructions used to generate the alterant tomograph in Fig. 9b were used as models to calculate noise-free synthetic data analogous to that collected in the field. Then, from this data, a second set of synthetic data was constructed by adding to it a normally distributed noise with measured standard deviation of the error estimates from the field data. These "noise-corrupted" and "noise-free" data sets were tomographically inverted. The effects of the original data errors on the tomographs were then estimated by subtracting, cell by cell, the "noise-corrupted" and "noise-free" tomographs. The standard deviation of these differences is an estimate of the 66 percent confidence level for any given reconstructed tomographic cell. The one standard deviation confidence level in an alterant tomograph (formed from two such error-corrupted tomographs with statistically independent errors) is $\sqrt{2}$ times the value for each. Figure 10b is the alterant tomograph of Fig. 9b with all image cells set to 0.0 m^{-1} change in attenuation rate whose value is less than two times the one standard deviation confidence level expected in this alterant image. In other words, Fig. 10b is the alterant tomograph in which the anomalies are at least two standard deviations larger than the image anomalies which we expect to be introduced by measurement errors. The results of this analysis have shown that the major image anomalies are not likely to be caused by random measurement error.

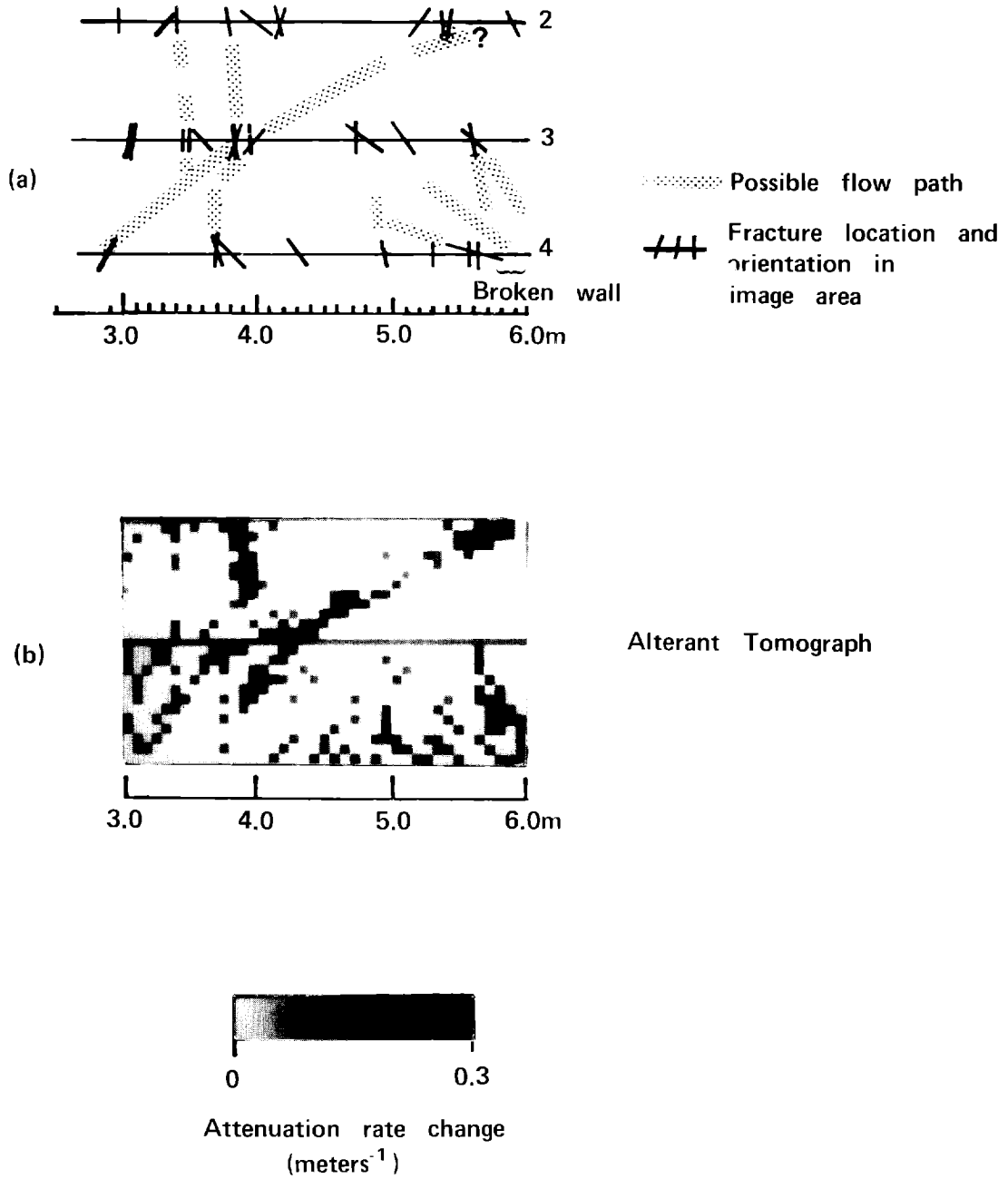

Figure 10. Comparison of available fracture orientation data (a) and the final alterant tomograph (b) in which any changes likely to be associated with random measurement errors (99% confidence level) have been set to 0.0 m^{-1}. Combining the borescope mapped fractures and the tomograph, possible flow paths have been postulated in (a). This analysis assumes that the lack of agreement between the dyed core data and the image anomalies is caused by drilling damage to the core.

4.5. Possible Flow Paths

The fracture locations mapped during the borescope surveys are shown in Fig. 9a. In addition, the orientation of most fractures in holes 2, 3, and 4 were estimated (reliable to approximately ± 20°) using the borescope. The orientation of these fractures as they would extend into the measurement plane is shown in Fig. 10a.

We have combined the fracture location and orientation data with the tomographic data to construct the model of possible flow paths in Fig. 10a. Note that the trends defined by the larger anomalies in Fig. 10a approximately match the orientation of fractures mapped with the borescope. In our judgment, this is the best of several models considered. However, we recognize that other possible models may explain the geophysical data. For example, the anomalies imaged in Fig. 10b may have been distorted by the tomographic algorithm (such as may be the case for the diagonal feature discussed later in this section). Thus, the set of possible flow paths presented in Fig. 10a should not be considered unique.

Other studies have documented that the resolution limits and inversion uniqueness of the geophysical tomography technique are a function of experimental geometry. Ramirez (1984) empirically illustrates the variations in the resolution which can be expected for various lineament orientations and experimental scenarios. Burkhard (1980) discusses the tradeoffs between resolving area, parameter contrast, cell size, and data accuracy. Menke (1984) analytically shows the resolution which can be expected for various experimental geometries.

From a comparison of borescope data and actual tomographs, we have reached several conclusions. These conclusions are presented on a tentative basis due to the absence of evidence (e.g., stained samples) conclusively correlating the image anomalies with tracer flow paths:

- This experiment has provided evidence concerning the applicability of alterant geophysical tomography to study flow paths in welded tuff. Positive indications of the technique's effectiveness are the lineal trends expected of fracture flow which are defined by the larger anomalies and the general agreement between the larger image anomalies in Fig. 10b and the orientation of some of the borescope--mapped fractures. At present, our judgment is that this type of correlation is more than coincidental. However, a large degree of uncertainty exists in our conclusions and observations due to the lack of recovered core to match most image anomalies. At present, we cannot conclusively determine whether this situation is indicative of the absence of tracer flow through the measurement region or whether drilling destroyed the stained fractures.

- As expected, there are anomalies which are nearly vertical. One anomaly suggestive of nonvertical flow paths is the prominent diagonal anomaly in the upper measurement region between 4 and 6 m depth. At present, we assume that this feature is caused by a discontinuous diagonal structure.

- Some of the possible flow paths are discontinuous; i.e., flow is not fully contained in the tomographic plane.

- The postulated flow paths of the tracer are associated with fractures (i.e., there is no evidence requiring matrix flow), but not all fractures serve as flow paths.

- Spatial resolution of the images appears to be about 7.5 cm (the size of a tomographic cell). For example, fractures along borehole 4 at depths of 3.7 and 4.1 meters appear to be represented in the image with a width equal to 1 cell size (7.5 cm).

5. SUMMARY AND CONCLUSIONS

In-situ electromagnetic measurements have been performed to evaluate the applicability of alterant geophysical tomography to delineate flow paths in fractured welded tuff. Computer simulation studies gave initial indications that this method might discriminate between the relatively large water content of the matrix (15-20 percent by volume), and the small amount of water flowing through fractures (less than 1 percent by volume). In-situ measurements of electromagnetic attenuation factor at 300 MHz have been made before, during, and after a water based dye tracer flowed through the rock mass. From these data alterant geotomographs were constructed and tracer flow paths were postulated. The following tentative conclusions can be reached based on evidence available at present:

- We have reported results from an experiment to evaluate alterant geophysical tomography for studying water flow in welded tuff. Parts of 3 image anomalies coincide with the location of dyed core, but the remaining anomalies exist where no dyed core was recovered. Either the unverified anomalies are erroneous, or the drilling process destroyed the dyed fracture faces. Additional investigations, including coring, are planned to evaluate these results.

- There is indirect evidence suggesting that the tomograph anomalies represent fracture flow. The large anomalies observed in the alterant tomographs coincide in orientation and location with fractures mapped by borescope surveys. Generally, mapped fractures can be matched with image anomalies which define lineal trends. The tomographic data is most useful when correlated with borescope fracture maps. Analyses of the propagation of measurement error in the alterant images have shown that the major image anomalies observed are caused by factors other than measurement noise.

Some additional uncertainties exist using geotomography for this application. The effects of rock mass stress and thermal gradients on the tomographs are unknown. We are also unsure whether water vapor can be detected by electromagnetic tomography.

The experiments in G-tunnel also identified several ideas important to the success of future work.

- Use of a rock stain to trace flow paths, for the most part, was disappointing. The drilling process as implemented damaged many of the fracture surfaces.

- The borescope logs yielded valuable data for fracture location which could be correlated with the tomographic data. However, from the borescope data alone, it was difficult to measure fracture orientation accurately and interpolate fractures between boreholes spaced only 30 cm apart, and it was impossible to tell which fractures would conduct water. Nevertheless, the value of correlating borescope and tomographic data suggests that the two techniques be used together in any attempt to map water flow in a rock mass.

- Several experimental parameters can be changed to improve the tomographs. Electrically short, nonresonant antennas should be used. Available evidence suggests that impedance changes of one antenna resulted in a bias in attenuation values calculated for the lower measurement region tomographs. Use of electrically short antennas could overcome this.

Electromagnetic phase as well as amplitude measurements could be advantageous so that both dielectric and attenuation tomographs can be made. The availability of both sets of data will add to confidence in inferring flow paths and could allow differentiation between liquid and vapor water. In

addition, smaller antennas and higher measurement frequency will allow improved spatial resolution in the tomographs.

ACKNOWLEDGEMENTS

The authors are grateful to R. J. Lytle, L. Ballou and E. F. Laine of Lawrence Livermore National Laboratory (LLNL) for invaluable advice and assistance. L. Ballou, R. J. Lytle, J. Yow, N. Burkhard and F. Heuze of LLNL reviewed this document and offered helpful suggestions which improved it. This experiment was made possible by the generous cooperation of several employees from Sandia National Laboratories. R. Zimmerman made available the experimental site and provided guidance during the planning stages of the experiment. We are particularly indebted to R. Schuch who provided support to our field activities. The cooperation of G. Hollis and E. Cooper from Reynolds Engineering Company is appreciated.

REFERENCES

Burkhard, N. R., Resolution and Error of the Back Projection Technique Algorithm for Geophysical Tomography, Lawrence Livermore National Laboratory, Livermore, CA, UCRL-52984, 1980.

Daily, W. D. and A. L. Ramirez, "In-Situ Porosity Distribution Using Geophysical Tomography," Geophy. Res. Letts., 11, No. 6, 614-616, 1984.

Daily, W. D, R. J. Lytle, E. F. Laine, J. T. Okada, and F. J. Deadrick, "Geotomography of Oil Shale," J. Geophys. Res., 87, 5507-5515, 1982.

Goodman, R. E., Introduction to Rock Mechanics, John Wiley & Sons, 1980.

Johnstone, K. J., and K. Wolfsberg (eds.), 1980, "Evaluation of Tuff as a Medium for Nuclear Waste Repository: Interim Status Report on the Properties of Tuff," Sandia National Laboratory, SAND 80-1464, Albuquerque, New Mexico, 1980.

Kuhl, D. E. and R. O. Edwards, "Image Separation Radioisotope Scanning," Radiology, V. 80, N. 4, 653-662, 1963.

Lager, D. L. and R. J. Lytle, "Determining a Subsurface Electromagnetic Profile from High-Frequency Measurements by Applying Reconstruction Technique Algorithms, Radio Science, V. 12, No. 2, 249-260, 1977.

Langkopf, B. S., and E. Eshom, "Site Exploration for Rock Mechanics Field Tests in the Grouse Canyon Member, Belted Range Tuff, U12g Tunnel Complex," Nevada Test Site, Sandia National Laboratory, SAND 81-1897, Albuquerque, New Mexico, 1982.

Lytle, R. J., "Effects of Boreholes and Tunnels on Antenna Radiation and Reception", Lawrence Livermore National Laboratory, UCRL-90834, submitted to the IEEE Trans. on Geoscience and Remote Sensing, May 1984.

Menke, W., "The Resolving Power of Cross-Borehole Tomography," Geophysical Research Letters, No. II, 105-109, 1984.

Poley, J. Ph., J. J. Nooteboom, and P. J. deWaal, "Use of VHF Dielectric Measurements for Borehole Formation Analysis," Log Analyst, May-June, 8-30, 1978.

Ramirez, A. L., "Inversion of Simulated Lineaments Using Geophysical Tomography," Lawrence Livermore National Laboratory, UCRL 91582, submitted to the International Journal of Rock Mechanics and Mining Services, September, 1984.

Ramirez, A. L., F. J. Deadrick and R. J. Lytle, "Cross-Borehole Fracture Mapping using Electromagnetic Geotomography," Lawrence Livermore National Laboratory, UCRL-53255, May 12, 1982.

Ramirez, A. L. and R. J. Lytle, "Alterant Geophysical Tomography," Lawrence Livermore National Laboratory , UCRL-89190, 1983.

Schuck, R., Personal Communication, Sandia National Laboratory, Albuquerque, NM.

Telford, W. M., L. P. Geldart, R. E. Sheriff and D. A. Keys, Applied Geophysics, Cambridge University Press, Cambridge, MA, 1976.

Winograd, G. J., and W. Thordarson, "Hydrogeologic and Hydrochemical Framework," Hydrology of Nuclear Test Sites, U. S. Geological Survey, Professional Paper 712-C, 1975.

APPENDIX

Consider the signal received by the two receiving antennas

$$\frac{P_1}{P_0} = \frac{f_{01}\, G_t\, A_1}{4\pi\, r_{01}^2}\, e^{-2\alpha_{01} r_{01}}$$

$$\frac{P_2}{P_1} = \frac{f_{02}\, G_t\, A_2}{4\pi\, r_{02}^2}\, e^{-2\alpha_{01} r_{01}}$$

where P_1 is the power received by antenna 1

P_2 is the power received by antenna 2

P_0 is the power radiated by the transmitter

f_{01} is the radiation pattern function for the transmitter and receiver 1

f_{02} is the radiation pattern function for the transmitter and receiver 2

G_t is the gain of the transmitting antenna

A_1 is the effective area of receiver 1

A_2 is the effective area of receiver 2

r_{01} is distance between transmitter and receiver 1

r_{02} is distance between transmitter and receiver 2

α_{01} is the effective attenuation rate between transmitter and receiver 1

α_{02} is the effective attenuation rate between transmitter and receiver 2

If the two receiving antennas are electrically identical then $f_{01} A_1 = f_{02} A_2$ and if the region is reasonably homogeneous electromagnetically so that $\alpha_{01} \sim \alpha_{02} \sim \alpha$ then

$$\frac{P_1}{P_2} = \left(\frac{r_{02}}{r_{01}}\right)^2 e^{-2\alpha(r_{01}-r_{01})}$$

Therefore, the electromagnetic properties of the rock are related only to measured power and the separations of the antennas, not to system parameters which are difficult to accurately determine.